

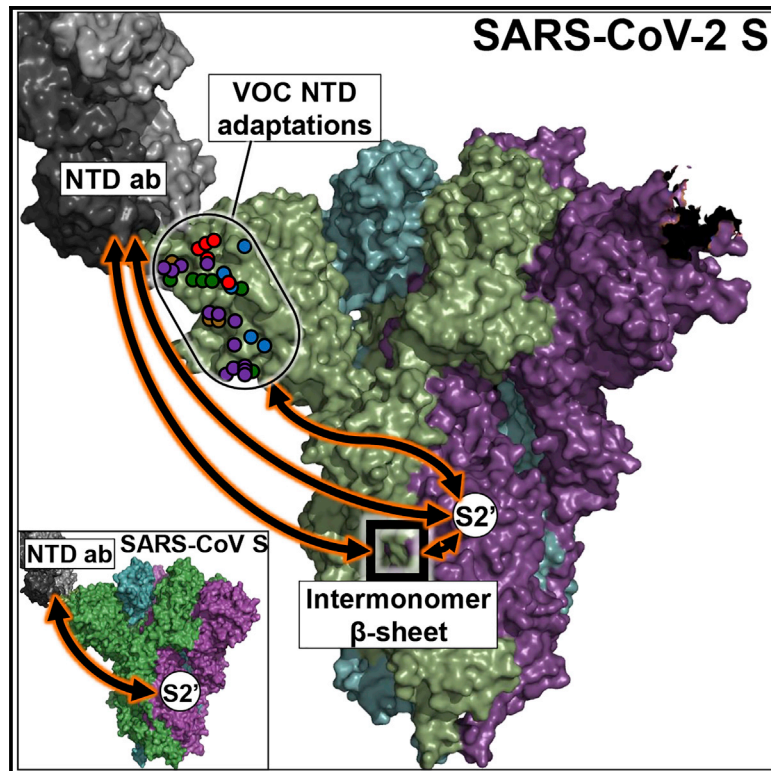


Since January 2020 Elsevier has created a COVID-19 resource centre with free information in English and Mandarin on the novel coronavirus COVID-19. The COVID-19 resource centre is hosted on Elsevier Connect, the company's public news and information website.

Elsevier hereby grants permission to make all its COVID-19-related research that is available on the COVID-19 resource centre - including this research content - immediately available in PubMed Central and other publicly funded repositories, such as the WHO COVID database with rights for unrestricted research re-use and analyses in any form or by any means with acknowledgement of the original source. These permissions are granted for free by Elsevier for as long as the COVID-19 resource centre remains active.

## Inter-domain communication in SARS-CoV-2 spike proteins controls protease-triggered cell entry

### Graphical abstract



### Authors

Enya Qing, Pengfei Li, Laura Cooper, ..., Lijun Rong, Stanley Perlman, Tom Gallagher

### Correspondence

tgallag@luc.edu

### In brief

Qing et al. identify connections between N-terminal and C-terminal domains of SARS-CoV-2 spike proteins that control the proteolytic activation of membrane fusion and show mechanisms of N-terminal domain-specific antibody neutralization.

### Highlights

- NTD-targeting antibodies block proteolytic activation of SARS-CoV-2 spike at S2'
- The NTD-to-S2' signaling is conserved in SARS-CoV spike
- An inter-monomer  $\beta$  sheet connects NTD ligation with proteolytic fusion activation
- SARS-CoV-2 VOC NTDs enhance sensitivity for proteolytic fusion activation



## Article

# Inter-domain communication in SARS-CoV-2 spike proteins controls protease-triggered cell entry

Enya Qing,<sup>1</sup> Pengfei Li,<sup>2</sup> Laura Cooper,<sup>3</sup> Sebastian Schulz,<sup>4</sup> Hans-Martin Jäck,<sup>4</sup> Lijun Rong,<sup>3</sup> Stanley Perlman,<sup>2</sup> and Tom Gallagher<sup>1,5,\*</sup>

<sup>1</sup>Department of Microbiology and Immunology, Loyola University Chicago, Maywood, IL 60153, USA

<sup>2</sup>Department of Microbiology and Immunology, University of Iowa, Iowa City, IA 52242, USA

<sup>3</sup>Department of Microbiology and Immunology, University of Illinois Chicago, Chicago, IL 60607, USA

<sup>4</sup>Division of Molecular Immunology, Friedrich-Alexander University Erlangen-Nuremberg and University Hospital Erlangen, 91054 Erlangen, Germany

<sup>5</sup>Lead contact

\*Correspondence: [tgallag@luc.edu](mailto:tgallag@luc.edu)

<https://doi.org/10.1016/j.celrep.2022.110786>

## SUMMARY

SARS-CoV-2 continues to evolve into variants of concern (VOC), with greatest variability in the multidomain, entry-facilitating spike proteins. To recognize the significance of adaptive spike protein changes, we compare variant SARS-CoV-2 virus particles in several assays reflecting authentic virus-cell entry. Virus particles with adaptive changes in spike amino-terminal domains (NTDs) are hypersensitive to proteolytic activation of membrane fusion, an essential step in virus-cell entry. Proteolysis is within fusion domains (FDs), at sites over 10 nm from the VOC-specific NTD changes, indicating allosteric inter-domain control of fusion activation. In addition, NTD-specific antibodies block FD cleavage, membrane fusion, and virus-cell entry, suggesting restriction of inter-domain communication as a neutralization mechanism. Finally, using structure-guided mutagenesis, we identify an inter-monomer  $\beta$  sheet structure that facilitates NTD-to-FD transmissions and subsequent fusion activation. This NTD-to-FD axis that sensitizes viruses to infection and to NTD-specific antibody neutralization provides new context for understanding selective forces driving SARS-CoV-2 evolution.

## INTRODUCTION

Even with available vaccines, antiviral treatments, and mitigation measures, SARS-CoV-2 continues to spread through human populations, with adaptive viruses becoming increasingly transmissible and potentially able to resist vaccine-induced immunity. Highly contagious variants of concern (VOC) emerge, first D614G, then  $\alpha$ ,  $\beta$ ,  $\gamma$ ,  $\delta$ , and  $\omicron$  variants. Conceivably a genetically stable variant with maximum transmissibility into both naive and immunized humans will eventually predominate (Burioni and Topol, 2021), yet this is not certain, making for current missions to predict ongoing SARS-CoV-2 evolutionary trajectories. Aims are in place to identify transmissibility determinants in past and current VOC and further elucidate VOC resistance to vaccine antibodies and antiviral agents. This study addresses a part of these aims by assessing VOC responses to host transmissibility determinants and by explicating antibody neutralization mechanisms.

VOC have acquired adaptive mutations throughout the ~30 kb RNA genome, yet most are present in the spike (S) gene. Variations in S proteins adapt viruses to diverse host factors conferring virus-cell entry. The principal host factors are receptors and proteases. Receptor binding domains (RBDs) adhere virus particles to target cell receptors, hence RBD mutations adapt vi-

ruses to human and animal orthologs of ACE2, the SARS-CoV-2 receptor (Niu et al., 2021; Ren et al., 2021; Wang et al., 2021b). Receptor-bound S proteins acquire conformations that are poised for membrane fusion (Benton et al., 2020; Jackson et al., 2022; Peng et al., 2021), and are then cleaved by host cell proteases to generate fragments that undergo large-scale multidomain conformational transitions. These transitory intermediate structures tether virus and cell membranes together and pull the two into coalescence (Jackson et al., 2022; Peng et al., 2021; Shang et al., 2020b). Mutations at or near protease cleavage sites increase or decrease spike fragmentation, in turn affecting proteolytic activation of membrane fusion (Hoffmann et al., 2020; Shang et al., 2020b; Walls et al., 2020). Other adaptive S protein mutations affect virus stability and fusion activation distinctly, for example, a powerfully selected D614G substitution in all VOC operates to stabilize S proteins in so-called “pre-fusion” conformations, increasing the durability of extracellular virus infectivity (Fernandez, 2020; Zhang et al., 2020, 2021a). Several more recently acquired VOC mutations alter epitopes, allowing viruses to escape neutralization by antibodies binding to RBDs and other domains (Gobeil et al., 2021; Graham et al., 2021; Planas et al., 2021; Wang et al., 2021a).

Amino-terminal domains (NTDs) of SARS-CoV-2 proteins are among the most hypervariable, with both indel and missense



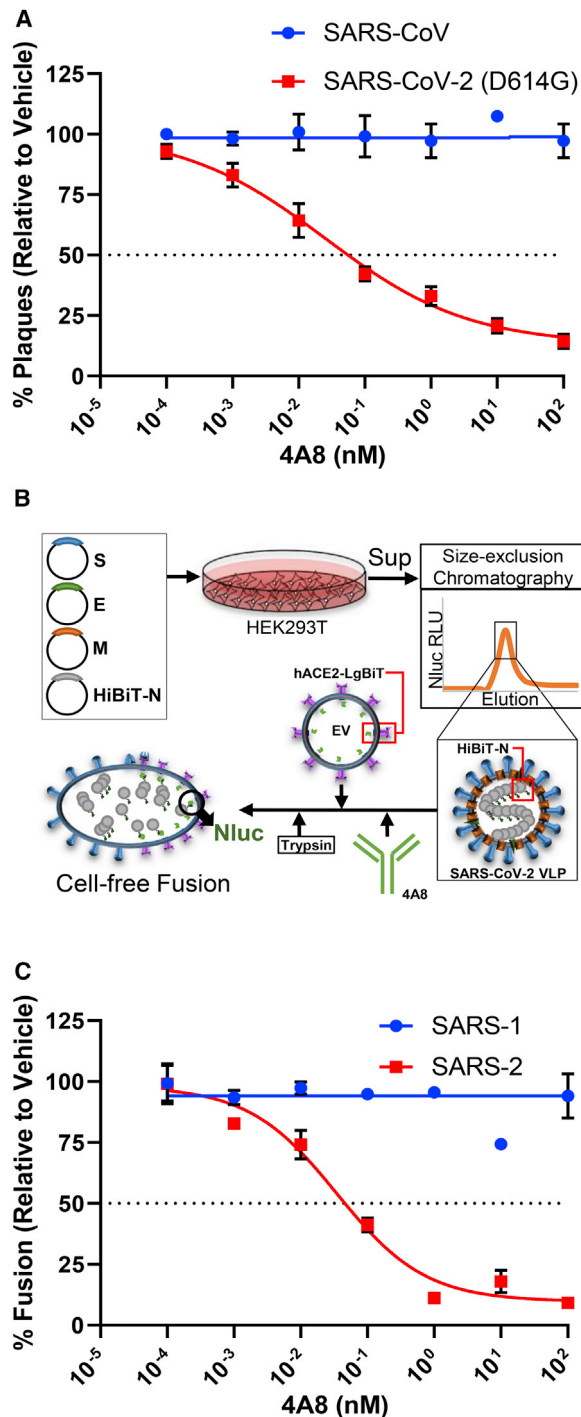


**Figure 1. NTD neutralizing antibodies block SARS-CoV-2 spike fusion**

(A) Authentic SARS-CoV or SARS-CoV-2(D614G) (SARS-1 or SARS-2, respectively) were incubated with titrated levels of antibody 4A8 before inoculating onto Vero-E6 cells. Plaques were counted at 48 hpi. Percent plaques was calculated relative to vehicle control.

(B) Schematic for VLP production and cell-free fusion. Supernatant from HEK293T cells expressing the SARS-CoV-2 structural proteins S, E, and M, and a HiBiT-tagged version of N (HiBiT-N) were harvested, and VLPs purified through size-exclusion chromatography. The effect of 4A8 on cell-free fusion

mutations in past and present VOC. This level of variation is puzzling in light of currently obscure NTD functions. While several studies suggest that the NTDs bind viruses to cellular ligands (Baker et al., 2020; Qing et al., 2021; Wei et al., 2020), the significance of these interactions is often unclear, as they cannot substitute for ACE2-directed virus-cell entry (Baker et al., 2020; Qing et al., 2021; Wei et al., 2020). In addition, the NTDs contain an “antigenic supersite” that is recognized by a prominent class of neutralizing antibodies (Cerutti et al., 2021; Graham et al., 2021; McCallum et al., 2021). This neutralization demonstrates the functional relevance of NTDs in virus entry, but the mechanism by which antibody binding to a domain apparently unnecessary for virus-cell binding or membrane fusion is hard to discern. Finally, there is the question of whether NTD variation is driven by a requirement for antibody escape. While it is definitely conceivable that variants overcoming antibody restriction are positively selected, the majority of acute SARS-CoV-2 infections take place within the unvaccinated (Cdcgov, 2021; Linsenmeyer et al., 2021; Muhsen et al., 2021; Ng et al., 2021; Singanayagam et al., 2022), raising the likelihood that VOC NTD variations offer fitness advantages that are independent of antibody evasion.

Here, we addressed these conundrums with novel *in vitro* systems that measure SARS-CoV-2 entry processes and their neutralization by NTD-specific antibodies. In discerning neutralization mechanisms, we discovered a functional linkage between NTDs and proteolytic substrate sites involved in fusion activation. NTD antibodies suppressed proteolytic activation of fusion. Selective pressures are exerted on this linkage, as VOC changes in the NTDs enhanced this proteolytic activation of fusion. The findings offer new insights into mechanisms of SARS-CoV-2 neutralization, and into contagious VOC that are hypersensitized to infection by host cell susceptibility factors.

## RESULTS

### NTD-specific antibodies neutralize authentic and virus-like SARS-CoV-2

SARS-CoV-2 NTD-specific antibodies bind to an antigenic supersite comprised of several projecting loops (Cerutti et al., 2021; McCallum et al., 2021; Suryadevara et al., 2021). These antibodies neutralize infections by unknown mechanisms. We expressed and purified several NTD-specific antibodies (Dodev et al., 2014; Peter et al., 2021). In initial tests, a prototype NTD mAb, 4A8 (Chi et al., 2020), was evaluated for neutralization of SARS-CoV and SARS-CoV-2 (D614G) cell entry. Consistent with previous studies (Chi et al., 2020; Wang et al., 2021a), 4A8 neutralized SARS-CoV-2 but not SARS-CoV (Figure 1A), as SARS-CoV spikes lack the loops comprising the NTD antigenic supersite (Cerutti et al., 2021; McCallum et al., 2021; Suryadevara et al., 2021).

between these VLPs and hACE2-LgBiT<sup>+</sup> EVs was detected by quantifying the Nluc activity arisen from HiBiT-LgBiT complementation.

(C) Cell-free fusion signal (relative to vehicle control) using SARS-1 or SARS-2 spike in the presence of titrated levels of NTD antibody 4A8. Mean and standard deviation (SD) (n = 3) are graphed. Data are representative of three biological repeats.

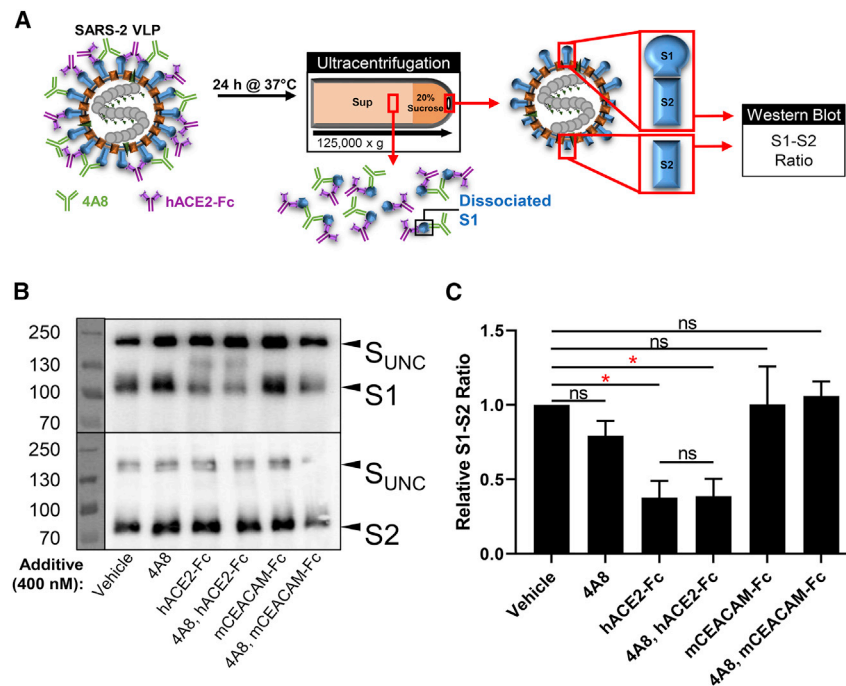


**Figure 2. NTD neutralizing antibodies do not affect spike S1-S2 stability**

(A) Schematic for VLP S1-retention assay. SARS-2 VLPs were pre-incubated with 4A8 and/or hACE2-Fc, or mCEACAM-Fc (not depicted) for 24 h at 37°C. VLPs were subsequently purified through 20% sucrose, and solubilized for western blot analysis of spike components.

(B) Western blot analysis of the resulted samples from VLP S1-retention assay. Samples for each condition were split into halves, one-half was probed with anti-S1 antibody while the other half with anti-S2 antibody. Uncleaved S ( $S_{UNC}$ ), S1, and S2 are labeled.

(C) The experiment from (B) was repeated three times, and the S1-S2 ratios (relative to vehicle control) were compared. Mean and standard error (SE) ( $N = 3$ ) are graphed. Significance was determined by one-way analysis of variance and multiple comparisons using Sidak test. ns, not significant; \* $p < 0.05$ .

To gain insights into the mechanisms by which 4A8 and other NTD-specific antibodies effect virus neutralization, we advanced into a more tractable *in vitro* model of virus-cell entry ((Qing et al., 2021); see Figure 1B). This assay system uses SARS-CoV-2 virus-like particles (VLPs) engineered to contain nanoluciferase (Nluc) “HiBiT” fragments. In the system, HiBiT VLPs are incubated with human ACE2-positive extracellular vesicles (EVs) that contain internal Nluc “LgBiT” fragments. Protease-triggered VLP-EV membrane fusions allow HiBiT and LgBiT to come together, generating the Nluc activities that are measured as readouts for spike protein-mediated membrane fusion.

SARS-CoV and SARS-CoV-2 VLPs induced robust Nluc signals upon incubation with EVs, with signals dependent on VLP spike proteins and on EV-associated hACE2 (Qing et al., 2021). In accord with the plaque reduction neutralization titers (PRNT) (Figure 1A), 4A8 antibodies neutralized fusion by SARS-CoV-2 (D614G) but not SARS-CoV, with anti-SARS-CoV-2 fusion titer equivalent to the PRNT values (Figure 1C). These findings validated the *in vitro* VLP-based assay system as an accurate reflection of authentic virus-cell entry and its neutralization.

### NTD-specific antibodies inhibit proteolytic cleavage of SARS-CoV-2 spike proteins

To address neutralization mechanisms, we first considered whether NTD antibodies interfere with an S1-S2 separation process that is traditionally taken as a measure of host cell receptor-induced conformational changes in CoV spike proteins (Gallagher, 1997; Matsuyama and Taguchi, 2009; Walls et al., 2019). This postulated antibody-mediated interference with S1-S2 stability was prompted by our prior discovery that the SARS-CoV-2 NTD “supersite” loops controlled S1 shedding from VLPs (Qing et al., 2021). SARS-2 VLPs were incubated with mAb 4A8, with or without soluble sarbeco (hACE2) recep-

tors, using soluble embeco (mCEACAM) receptors as negative controls. VLPs were then pelleted free of shed S1 and evaluated for S1-S2 ratios (Figure 2A). As expected, hACE2 but not mCEACAM receptors caused S1 shedding (Figures 2B and 2C). Notably, 4A8 mAbs did not suppress the hACE2-induced shedding (Figures 2B and 2C), indicating that the mAbs do not neutralize by disturbing virus-receptor binding or resultant spike protein conformational changes leading to heterodimer destabilization.

We next asked whether NTD antibodies interfere with the spike proteolytic cleavages that are essential prerequisites for virus-cell membrane fusion (Hoffmann et al., 2018; Matsuyama and Taguchi, 2009; Millet and Whittaker, 2018; Park et al., 2016). We previously demonstrated that SARS-2 VLP fusion with hACE2<sup>+</sup> EVs is associated with proteolysis at the well-characterized S2' position (Qing et al., 2021). With 4A8 mAb in the VLP-EV fusion reactions (Figure 3A), S2' cleavages were notably suppressed (Figure 3B), clearly distinct from control isotype Fc proteins that exerted no effect on S2' cleavage (Figure S1). Reduced S2' cleavage correlated precisely with diminished membrane fusion (Figure 3C). An independently identified NTD antibody TRES328 (Peter et al., 2021) phenocopied 4A8 in S2' cleavage and fusion inhibition (Figure S2), suggesting a common neutralization mechanism for the NTD antibodies. Replacement of the VLPs with authentic SARS-CoV-2 (D614G) particles gave similar results, showing that 4A8 mAbs suppressed S2' cleavage (Figures 3D and 3E). These results indicate that NTD-binding antibodies neutralize SARS-CoV-2 spike by blocking S2' cleavage.

We also determined whether the relays from NTDs to S2' cleavage sites are present in SARS-CoV spikes. Here, we spliced the SARS-CoV-2 NTD loops into SARS-CoV spikes, effectively constructing the SARS-CoV-2 antigenic supersite onto SARS-CoV (Qing et al., 2021) (see Figure S3). VLPs with these engineered SARS-CoV spikes elicited membrane fusions that were effectively suppressed by 4A8 mAbs, while fusions generated by standard SARS-CoV VLPs were unaffected (Figures 4A and 4B).

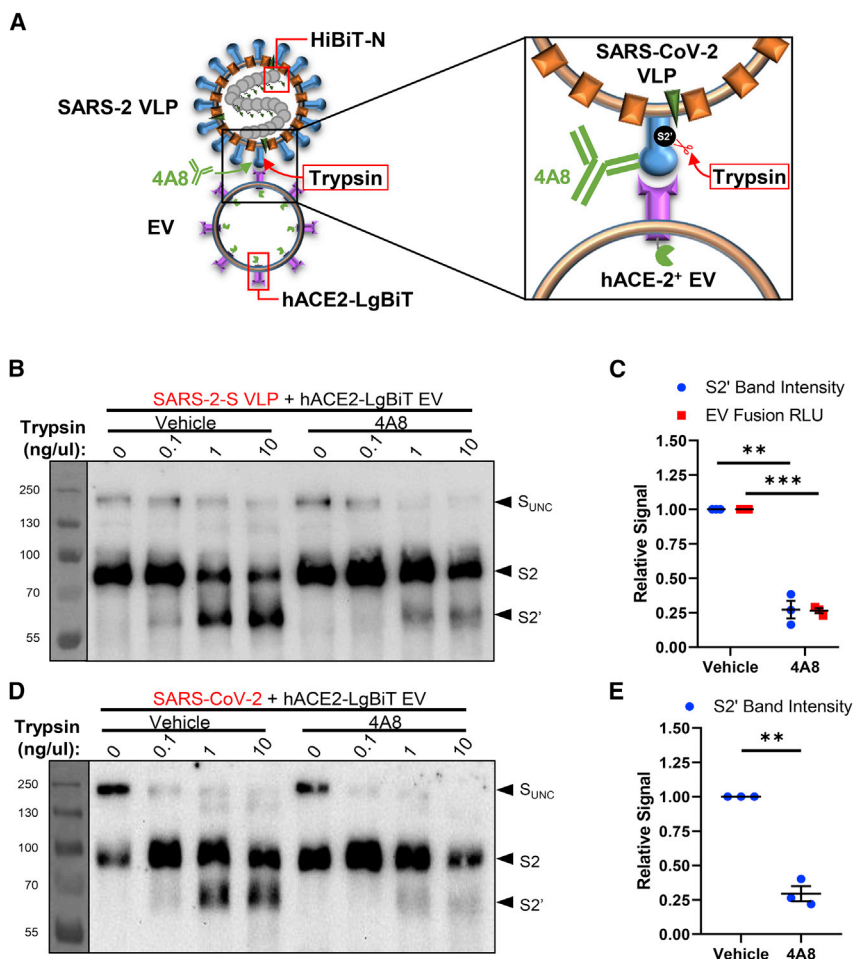


**Figure 3. NTD neutralizing antibodies block SARS-CoV-2 spike fusion at S2' cleavage**

(A) Schematic for S2' cleavage assay. SARS-2 VLPs, pre-incubated with vehicle or 4A8, were mixed with hACE2-LgBiT EVs. Membrane fusion was subsequently activated by titrated levels of trypsin, which cleaves at the spike S2' position. The resulted mixture was split and analyzed for both its generation of S2' cleavage product via western blot and membrane fusion via Nluc activity.

(B) SARS-2-S VLPs were sequentially incubated with vehicle or 4A8, hACE2-LgBiT EV, and the indicated amounts of trypsin for 30 min each at 37°C, before being solubilized for western blot (WB) analysis of S2 cleavage patterns. The position of the S2' proteolytic product is indicated.

(C) The experiment from (B) was repeated three times, and the S2' band intensities at 10 ng/μL trypsin were compared with their corresponding cell-free fusion signals. Mean and SE (N = 3) are graphed.

(D) SARS-CoV-2 (D614G) virus were sequentially incubated with vehicle or 4A8, hACE2-LgBiT EV, and the indicated amounts of trypsin for 30 min each at 37°C, before being solubilized for WB analysis of S2 cleavage patterns. The position of S2' proteolytic product is indicated.

(E) The experiment from (D) was repeated three times, and the S2' band intensities at 10 ng/μL trypsin were compared. Mean and SE (N = 3) are graphed. Significance was determined by one-sample t test. ns, not significant; \*\*p < 0.01, \*\*\*p < 0.001. See also Figures S1, S2, and S8.

Membrane fusion levels correlated precisely with the extents of S2' cleavage (Figures 4C and 4D). These results suggest that the communications between NTDs and S2' cleavage sites are conserved in the sarbecoviruses, and that neutralizing antibodies interfere with NTD mobility such that fusion domains (FDs) remain uncleaved and incompetent in virus entry.

### Substitutions at inter-domain locations hypersensitize viruses to NTD antibody neutralization

In pre-fusion spike trimers, the NTD antigenic supersites are about 10 nm from the nearest S2' cleavage sites (Figure 5A). Furthermore, NTDs are not present in currently available post-fusion spike trimer structures (Cai et al., 2020; Liu et al., 2020), and so it is not obvious how NTD positioning or restricted NTD mobility might expose or conceal a distal protease substrate site. To gain insights into the structures linking NTD position to S2' cleavage, we used molecular genetic approaches, asking whether SARS-CoV-2 spike variations might promote or impede NTD mAb neutralization. We started with naturally occurring variations. These included a D614G substitution that stabilizes SARS-CoV-2 spikes (Qing et al., 2021; Zhang et al., 2020), affects RBD up-down transitions (Yurkovetskiy et al., 2020), and increases viral transmissibility (Hou et al., 2020; Volz et al., 2021)

and attenuates SARS-CoV-2 *in vivo* (Chu et al., 2021; Johnson et al., 2021; Lau et al., 2020; Peacock et al., 2021) (Figure S4). Neither of these spike variations effected changes to VLP fusion activation and its neutralization by 4A8 mAbs.

Guided by a hypothesis that inter-monomer rearrangements expose S2' sites for proteolytic activation (Gobeil et al., 2021), we continued analyses with two changes, N317A and D737A, that disrupt an inter-domain bridge residing near the apex of S2 (Figure 5B). This N317-D737 bridge is near the well-known "2P" (K986P/V987P) changes that stabilize pre-fusion spikes (McCallum et al., 2021; Walls et al., 2020; Wrapp et al., 2020), which, perhaps expectedly, prevented S2' cleavage (Figure S5). Also evaluated were D796H/Y changes that disrupt an inter-domain D796-Y707 bridge (Figure 5C) and were reported to operate allosterically in conferring virus resistance to neutralization by convalescent patient sera (Kemp et al., 2021). Neither the N317A/D737A nor the D796H/Y substitutions effected changes to VLP fusion activation and its neutralization by 4A8 mAbs (Figures 5B and 5C). Holding to the hypothesis that inter-monomer rearrangements expose S2' cleavage sites, we continued the search for functional links between NTDs and S2' cleavage sites and noted a β sheet comprised of strands from two adjacent monomers; residues 701–705 (green) adjacent to residues

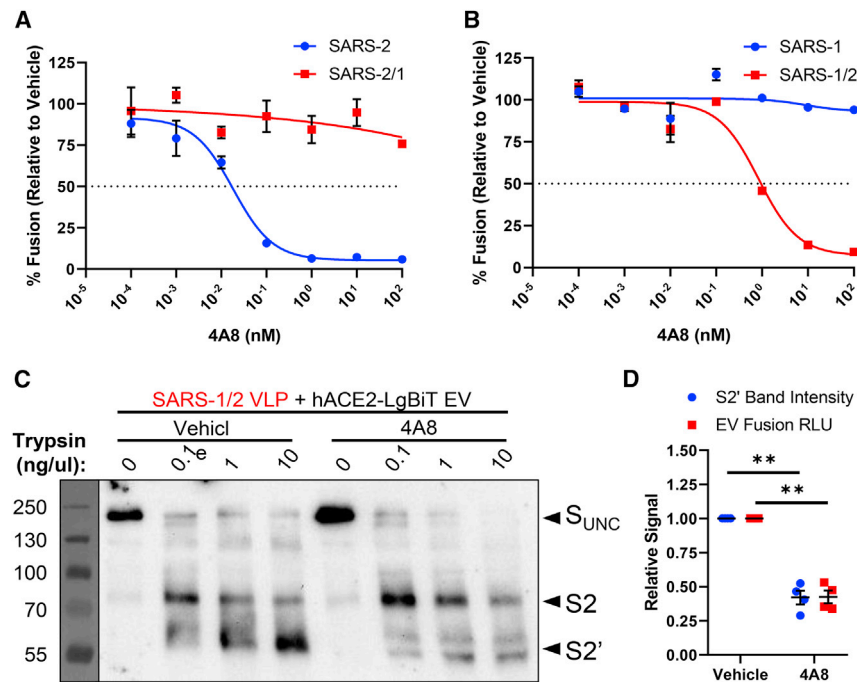


**Figure 4. The NTD-S2' functional axis is conserved in the SARS-CoV spike**

(A and B) Cell-free fusion signal (relative to vehicle control) using SARS-2 or SARS-2/1 (A) and SARS-1 or SARS-1/2 (B) spike VLPs in the presence of titrated levels of NTD antibody 4A8. Mean and SD (n = 3) are graphed. Data are representative of three biological repeats.

(C) SARS-1/2-S VLPs were sequentially incubated with vehicle or 4A8, hACE2-LgBiT EV, and the indicated amounts of trypsin for 30 min each at 37°C, before being solubilized for WB analysis of S<sub>2</sub> cleavage patterns. The position of S<sub>2</sub>' proteolytic product is indicated.

(D) The experiment from (C) was repeated four times, and the S<sub>2</sub>' band intensities at 10 ng/μL trypsin were compared with their corresponding cell-free fusion signals. Mean and SE (N = 4) are graphed. Significance was determined by one-sample t test. \*\*p < 0.01. See also [Figures S3 and S8](#).

787–790 (magenta) with inter-monomer stabilization achieved by A701/N703 interactions with I788 ([Figure 5D](#)). These strands are near the S<sub>2</sub>' cleavage sites ([Figure 5A](#)). We introduced β strand-disrupting A701P and N703P substitutions into VLPs. Here, VLPs with these substitutions were nearly 10-fold more sensitive to mAb 4A8 neutralization ([Figure 5D](#)). This hypersensitivity to NTD mAb neutralization suggested that the proline substitutions facilitated NTD-driven S<sub>2</sub>' cleavage and fusion activation. Using trypsin titrations to assess fusion triggering, we found that the A701P/N703P VLPs were indeed activated for fusion at trypsin levels that were nearly 10-fold lower than wild-type (WT) VLPs ([Figures 5D and S6](#)). These findings identify an inter-monomer β sheet “linker,” between NTDs and FDs, that is involved in transmitting NTD ligation signals to FDs. The results further document a remarkable concordance between NTD mAb neutralization sensitivity and proteolytic triggering of viral membrane fusion.

### The NTD changes in VOC increase sensitivity to protease-triggered membrane fusion

In SARS-CoV-2 VOC, there are substitution mutations in RBDs, in S1-S2 furin cleavage sites, in FDs, and notably also in the NTDs ([Davies et al., 2021](#); [Faria et al., 2021](#); [Tegally et al., 2021](#); [Zhang et al., 2021b](#)). Many of the NTD changes are within the antigenic supersite ([Figure 6A](#)) and, expectedly, several VOC are resistant to neutralization by NTD antibodies ([Cai et al., 2021](#); [Gobeil et al., 2021](#); [Graham et al., 2021](#); [Planas et al., 2021](#); [Wang et al., 2021a](#)). However, it is not known whether the NTD changes also impact virus entry properties independent of antibody escape. Based on our prior understanding of NTD deletions and their profound effects on virus stability ([Qing et al., 2021](#)) and on our newly identified functional links between NTD supersites and S<sub>2</sub>' cleav-

(WT) spike background and generated VOC spike-containing VLPs. We then utilized cell-free VLP-EV fusion assays to identify requirements for protease-triggered membrane fusion. Relative to the “WT” VLPs, all five VOC VLPs were hypersensitive to trypsin protease-triggered fusion ([Figures 6B–6G](#)). Furthermore, VOC VLPs showed relatively sharp trypsin dose-response profiles ([Figures 6C–6F](#)), suggesting cooperativity in fusion-activating spike proteolysis ascribed to the NTD alterations. Of note, these VOC-specific NTD changes that are distant from proteolytic cleavage sites increase susceptibility to host cell proteases similarly to the more proximal 701P/703P changes ([Figure 5D](#)), consistent with a long-distance activation relay from NTD-to-FDs. The overall findings make a case for host proteases as driving forces for spike protein NTD adaptations, with the NTD changes contributing to the high transmissibility of VOC.

### DISCUSSION

In visualizing coronavirus binding to susceptible host cells and resultant virus-cell membrane fusion and cell entry, one can look to virus particle “pre-fusion,” receptor-bound “intermediate” and “post-fusion” end-stage spike structures ([Benton et al., 2020](#); [Cai et al., 2020](#); [Walls et al., 2020](#)). Further dissecting the controlled transitions between these structural states is central to understanding coronavirus entry and its therapeutic inhibition ([Jackson et al., 2022](#); [Peng et al., 2021](#)). In working toward this added perception, antibodies are frequently employed to capture and subsequently resolve structural intermediates ([Chi et al., 2020](#); [McCallum et al., 2021](#); [Wang et al., 2022](#); [Yang et al., 2021](#)). Here, we used SARS-CoV-2 neutralizing antibodies to probe the conformational transitions leading to spike proteolytic cleavages and virus-cell membrane fusion. Using

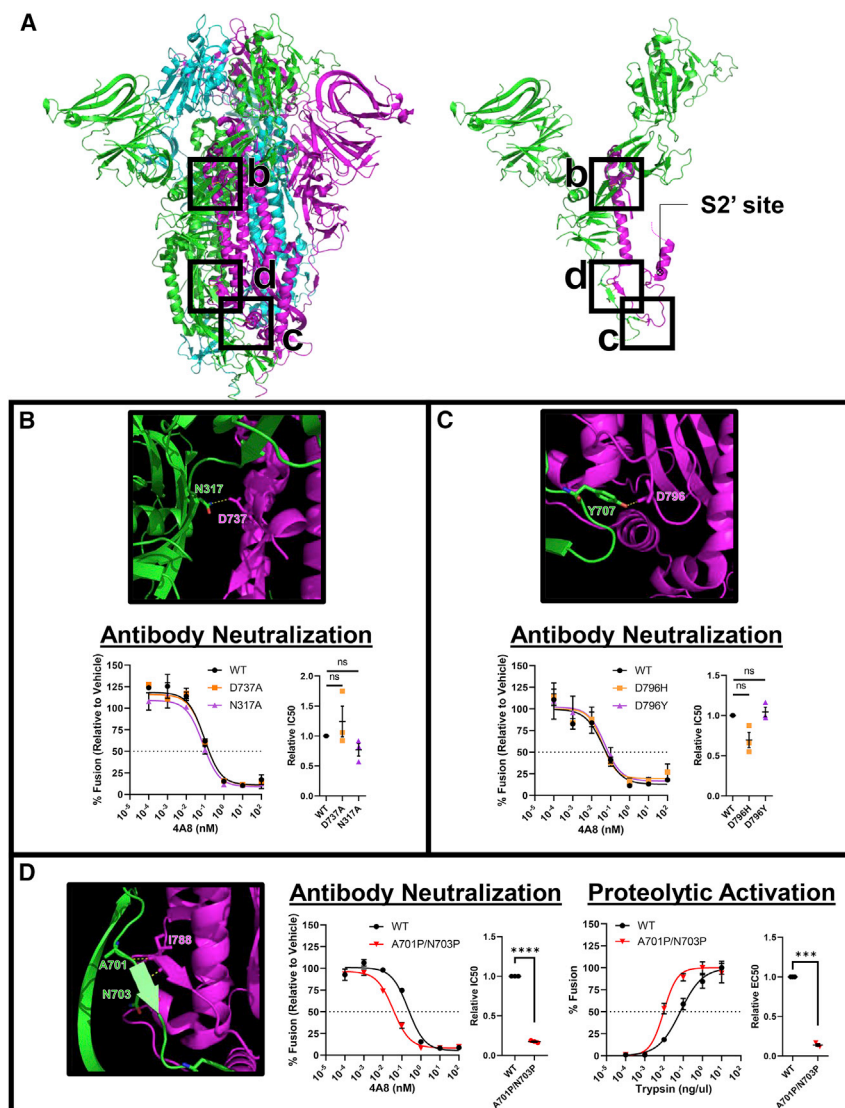


**Figure 5. An S2'-proximal region on the neighboring S monomer augments NTD-mediated neutralization**

(A) Left: ribbon diagram of SARS-CoV-2 spike (PDB: 7LXY), where each S monomer is colored (green, magenta, and cyan). Right: ribbon diagram with certain S trimer elements omitted for clarity. The S2' proteolytic site is indicated. Regions highlighted in (B–D) are indicated by black boxes.

(B–D) Structure: zoomed-in regions of the boxed areas from (A). The vantage points are rotated slightly to distinguish the highlighted interactions. Certain structural elements of the S trimer are omitted for clarity. Antibody neutralization: (left) cell-free fusion signal (relative to vehicle control) from VLPs bearing the indicated spikes in the presence of titrated levels of NTD antibody 4A8. Mean and SD (n = 3) are graphed. (Right) The experiment from the left panel was repeated three times, and the IC<sub>50</sub> values (relative to WT) were compared. Mean and SE (N = 3) are graphed. Proteolytic activation: (left) cell-free fusion signal (relative to maximum fusion) from VLPs bearing the indicated spikes in the presence of titrated levels of trypsin. Mean and SD (n = 3) are graphed. (Right) The experiment from the left panel was repeated three times, and the EC<sub>50</sub> values (relative to WT) were compared. Mean and SE (N = 3) are graphed. For (B) and (C), significance was determined by one-way analysis of variance and multiple comparisons using Dunnett's test. For (D), significance was determined by one-sample t test. ns, not significant; \*\*\*p < 0.001, \*\*\*\*p < 0.0001. See also Figures S4, S5, S6, and S9.

antibodies specifically binding to distal NTDs of the spike proteins, we identified links between NTD ligation and a virus entry-activating proteolytic event taking place at distant "S2'" locations within the FDs. The discovery of this NTD-to-S2' signaling clarifies our vision of coronavirus-cell entry and provides insights on the nature of concerning SARS-CoV-2 variations.

The neutralization mechanisms were elucidated using a tractable *in vitro* virus-cell membrane fusion system that reflects authentic SARS-CoV-2 entry (Qing et al., 2021). Using this system, we demonstrated that NTD antibodies did not interfere with virus binding to hACE2 receptors, nor did they suppress an S1-S2 separation process that arises subsequent to hACE2 binding (Chi et al., 2020; McCallum et al., 2021; Suryadevara et al., 2021) (Figures 2B and 2C). Rather, the antibodies blocked S2' cleavage. The *in vitro* fusion system revealed a striking concordance between S2' cleavage and membrane fusion (Figure S8), making it abundantly clear that the essential requirement for virus fusion and cell entry is in liberating the S2' transmembrane cleavage

a near end-stage S1 separation occurring regardless of whether the spikes execute productive membrane fusion. This is distinct from previous models depicting viruses engaging receptors and then undergoing complete separation from S1 fragments to reveal underlying S2 domains, which are then cleaved at S2' to allow for spike refolding in concert with virus-cell membrane fusion (Jackson et al., 2022; Peng et al., 2021).

The revised entry model prompted us to identify structural elements communicating a suppressive signal from S1 NTDs to S2 FDs. One of three elements evaluated was a  $\beta$  sheet spanning two spike monomers (Figure 5D). Disrupting this  $\beta$  sheet with proline substitutions heightened virus sensitivity to NTD antibody neutralization and to protease-activated membrane fusion. This inter-domain  $\beta$  sheet element may be one of several hubs controlling responses to signals emanated by NTD- or RBD-binding ligands. These signal-transducing elements may be central to sarbecoviruses, as S2' cleavage and membrane fusion by the related SARS-CoV spikes were also suppressed

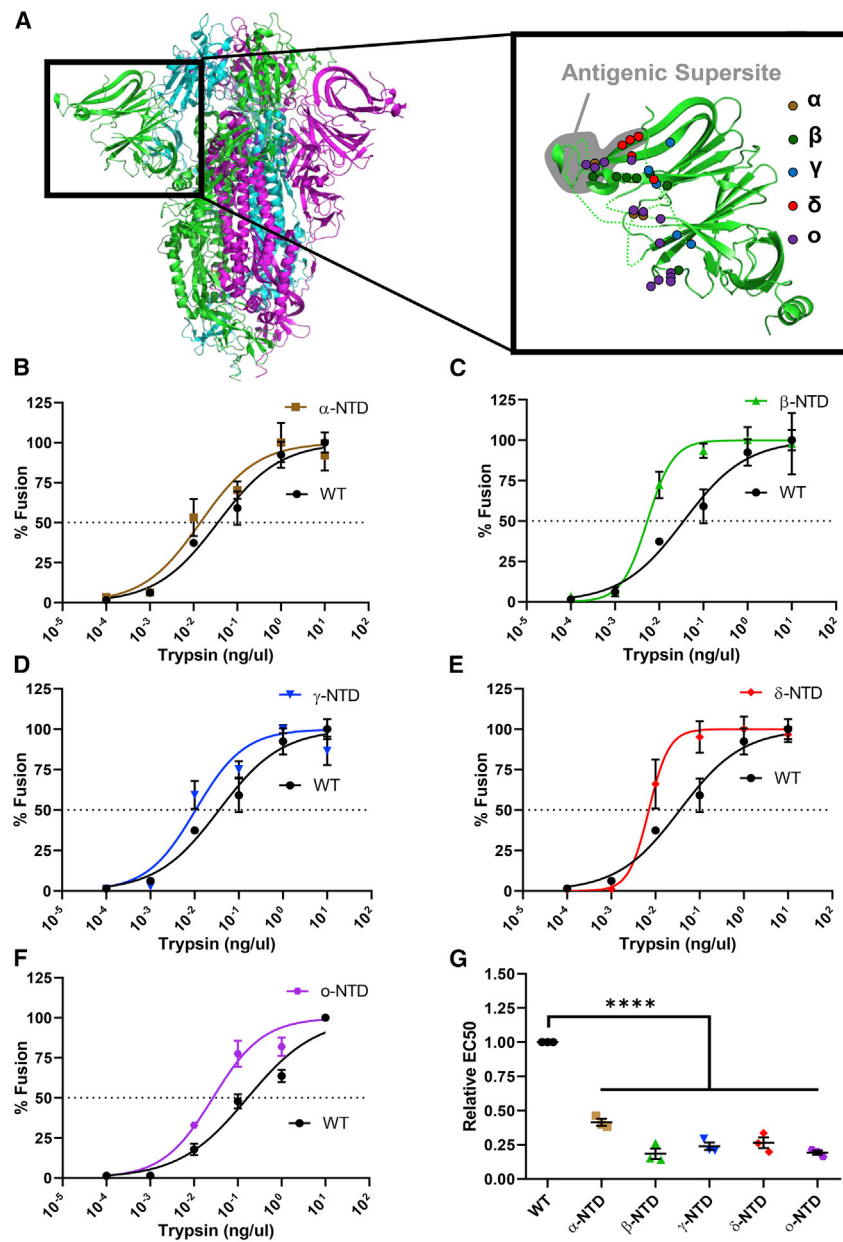


**Figure 6. SARS-CoV-2 VOC NTD mutations enhance S protein sensitivity to proteolytic activation**

(A) Left: ribbon diagram of the SARS-CoV-2 spike (PDB: 7LXY), where each S monomer is colored (green, magenta, and cyan). Right: enlarged NTD of one S monomer. The antigenic supersite for NTD neutralizing antibodies is shaded in gray. The locations of NTD mutations in each SARS-CoV-2 VOC are marked by colored dots.

(B–F) Cell-free fusion signal (relative to maximum fusion) using the SARS-2 spike with NTDs from WT or  $\alpha$  (B),  $\beta$  (C),  $\gamma$  (D),  $\delta$  (E), or o (F) VOC in the presence of titrated levels of trypsin. Mean and SD (n = 3) are graphed.

(G) Experiments from (B–F) were repeated three times, and their EC<sub>50</sub> values (relative to WT NTD) were compared. Mean and SE (N = 3) are graphed. Significance was determined by one-way analysis of variance and multiple comparisons using Holm-Sidak test. \*\*\*\*p < 0.0001. See also Figure S7.

by NTD ligation (Figure 4). Importantly, the NTDs of several coronaviruses are bona fide “RBDs,” with receptor ligation activating cell entry. Among these are the embecoviruses, which are activated for fusion following NTD binding to Ig-like CEACAM receptors (Godfraind et al., 1995; Hensley et al., 1998; Shang et al., 2020a). How CEACAM binding to embecovirus NTDs elicits fusion while IgG antibody binding to sarbecovirus NTDs suppresses fusion is currently unclear, yet it is notable the prototype embecovirus MHV lacks the suppressive sarbecovirus  $\beta$  sheet element (Figure S9). Conceivably the adaptive restructuring of signaling hubs allows NTDs to operate as primary RBDs. Several ligands unrelated to hACE2 are known to bind to SARS-CoV-2 NTDs (Baker et al., 2020; Lempp et al., 2021; Wei et al., 2020)

and there are reports of hACE2-independent entry of SARS-CoV-2 (Puray-Chavez et al., 2021), raising the possibility that additional adaptations in the SARS-CoV-2 NTD-to-S2’ axis could generate variants that employ the NTDs as full-fledged RBDs that stimulate rather than suppress S2’ cleavage and fusion. Adaptive evolution of SARS-CoV-2 is proceeding throughout the COVID19 pandemic, with VOC arising and replacing prior versions. Neutralizing antibodies are frequently proposed as selective agents in driving adaptive VOC changes in spike proteins (McCallum et al., 2021; Planas et al., 2021; Wang et al., 2021a), and VOC changes, particularly those in the NTDs, do indeed confer antibody escape (Cai et al., 2021; Graham et al., 2021; Planas et al., 2021; Wang et al., 2021a). However, given that most human hosts have been immunologically naive and unlikely to select for antibody-resistant viruses during acute infection periods, alternative selective forces may be central in driving spike variations. As interference with NTD dynamics suppressed viral fusion, we asked whether VOC NTD changes are adaptive in entry processes, and we found that NTD changes from  $\alpha$ ,  $\beta$ ,  $\gamma$ ,  $\delta$ , and o VOC all increased virus sensitivity for proteolytic activation of membrane fusion (Figures 6B–6G). Therefore, we suggest that the NTD adaptations contribute, along with additional VOC changes in other spike domains, to promote SARS-CoV-2 transmissibility into host environments that have trypsin-like serine proteases, such as TMPRSS2, and/or endosomal proteases, such as cathepsin L. These environments include the nasal epithelia, with ciliated cells presenting TMPRSS2 apically into airway spaces (Ahn

et al., 2021; Chu et al., 2021; Muus et al., 2021; Nakayama et al., 2021). Whether protease levels exert selective pressures greater or lesser than neutralizing antibodies is unknown, as the VOC changes analyzed here confer both antibody escape and proteolytic sensitivity. Yet selection at the level of proteolytic activation is strongly supported by recent analyses of the omicron variant, which exhibits distinctive preferences for cathepsin proteases over the prior VOC that are adapted to TMPRSS2 (Willett et al., 2022). It is important to note that the findings in this report do not explain differential VOC preferences for distinct activating proteases, nor do they indicate whether distinct NTD changes account for the continuing cycles of new VOC emergence and dominance. Undoubtedly many combinations of VOC changes outside of the NTD contribute in complex ways, particularly for the omicron variant that is set apart in its cell entry (Peacock et al., 2022). Adaptive changes beyond the spikes are also relevant, and it will require worldwide research efforts to obtain a complete atlas of the SARS-CoV-2 variations affecting virus pathogenesis, transmissibility, and neutralization.

### Limitations of the study

Only two NTD-specific antibodies were evaluated in this study. Whether additional neutralizing antibodies operate by suppressing proteolytic activation of membrane fusion remains to be determined. An NTD-to-FD axis was recognized in this study, yet NTD variations may also control NTD-to-RBD communications. NTD variations alter spike protein functions in concert with changes in other domains and this complexity requires additional comparisons with viruses harboring RBD and FD changes. Finally, in this study, the effects of amino acid substitutions on NTD-to-FD communication were evaluated using cell-free fusion assays. The impact of these changes during natural virus-cell entry remains to be determined.

### STAR★METHODS

Detailed methods are provided in the online version of this paper and include the following:

- **KEY RESOURCES TABLE**
- **RESOURCE AVAILABILITY**
  - Lead contact
  - Materials availability
  - Data and code availability
- **EXPERIMENTAL MODEL AND SUBJECT DETAILS**
  - Cell lines
  - Viruses
- **METHOD DETAILS**
  - Plasmid construction
  - Western blot and antibodies
  - Plaque reduction assay
  - Virus-like particles (VLPs)
  - Cell-free fusion assay
  - VLP S1-retention assay
  - S2' cleavage assay
  - Fc constructs
- **QUANTIFICATION AND STATISTICAL ANALYSIS**

### SUPPLEMENTAL INFORMATION

Supplemental information can be found online at <https://doi.org/10.1016/j.celrep.2022.110786>.

### ACKNOWLEDGMENTS

Major support for this study was provided by the National Institutes of Health (NIH) under award P01 AI060699 (to T.G. and S.P.). Additional support was provided by grants TRR130 and GRK1660 from Deutsche Forschungsgemeinschaft (DFG), grants 01KI2043 and COVIM (NaFoUniMedCovid19; FKZ: 01KX2021) from the Bundesministerium für Bildung und Forschung (BMBF), and grants from the Bayerische Forschungsstiftung and the Bavarian Ministry of Art and Science (to H.-M.J.).

### AUTHOR CONTRIBUTIONS

Conceptualization, E.Q. and T.G.; methodology, E.Q. and T.G.; investigation, E.Q., P.L., L.C., and S.S.; resources, P.L., L.C., S.S., H.-M.J., L.R., and S.P.; writing – original draft, E.Q. and T.G.; writing – review & editing, E.Q., H.-M.J., L.R., S.P., and T.G.; funding acquisition, T.G. and S.P.; supervision, H.-M.J., L.R., S.P., and T.G.

### DECLARATION OF INTERESTS

The authors declare no competing interests.

Received: February 1, 2022

Revised: March 11, 2022

Accepted: April 13, 2022

Published: May 3, 2022

### REFERENCES

- Ahn, J.H., Kim, J., Hong, S.P., Choi, S.Y., Yang, M.J., Ju, Y.S., Kim, Y.T., Kim, H.M., Bae, H., Lee, C.S., et al. (2021). Nasal ciliated cells are primary targets for SARS-CoV-2 replication in the early stage of COVID-19. *J. Clin. Invest.* *131*, e148517. <https://doi.org/10.1172/JCI148517>.
- Baker, A.N., Richards, S.J., Guy, C.S., Congdon, T.R., Hasan, M., Zwetsloot, A.J., Gallo, A., Lewandowski, J.R., Stansfeld, P.J., Straube, A., et al. (2020). The SARS-COV-2 spike protein binds sialic acids and enables rapid detection in a lateral flow point of care diagnostic device. *ACS Cent. Sci.* *6*, 2046–2052. <https://doi.org/10.1021/acscentsci.0c00855>.
- Benton, D.J., Wrobel, A.G., Xu, P., Roustan, C., Martin, S.R., Rosenthal, P.B., Skehel, J.J., and Gamblin, S.J. (2020). Receptor binding and priming of the spike protein of SARS-CoV-2 for membrane fusion. *Nature* *588*, 327–330. <https://doi.org/10.1038/s41586-020-2772-0>.
- Burioni, R., and Topol, E.J. (2021). Has SARS-CoV-2 reached peak fitness? *Nat. Med.* *27*, 1323–1324. <https://doi.org/10.1038/s41591-021-01421-7>.
- Cai, Y., Zhang, J., Xiao, T., Lavine, C.L., Rawson, S., Peng, H., Zhu, H., Anand, K., Tong, P., Gautam, A., et al. (2021). Structural basis for enhanced infectivity and immune evasion of SARS-CoV-2 variants. *Science* *373*, 642–648. <https://doi.org/10.1126/science.abi9745>.
- Cai, Y., Zhang, J., Xiao, T., Peng, H., Sterling, S.M., Walsh, R.M., Jr., Rawson, S., Rits-Volloch, S., and Chen, B. (2020). Distinct conformational states of SARS-CoV-2 spike protein. *Science* *369*, 1586–1592. <https://doi.org/10.1126/science.abd4251>.
- Cdcgov. (2021). Incidence of SARS-CoV-2 infection, emergency department visits, and hospitalizations because of COVID-19 among persons aged ≥ 12 years, by COVID-19 vaccination status – Oregon and Washington, July 4–September 25, 2021. *MMWR*. @CDCMMWR. 2021-11-17T11:08:04Z. <https://www.cdc.gov/mmwr/volumes/70/wr/mm7046a4.htm>.
- Cerutti, G., Guo, Y., Zhou, T., Gorman, J., Lee, M., Rapp, M., Reddem, E.R., Yu, J., Bahna, F., Bimela, J., et al. (2021). Potent SARS-CoV-2 neutralizing antibodies directed against spike N-terminal domain target a single supersite.

Cell Host Microbe 29, 819–833.e7. <https://doi.org/10.1016/j.chom.2021.03.005>.

Chi, X., Yan, R., Zhang, J., Zhang, G., Zhang, Y., Hao, M., Zhang, Z., Fan, P., Dong, Y., Yang, Y., et al. (2020). A neutralizing human antibody binds to the N-terminal domain of the Spike protein of SARS-CoV-2. *Science* 369, 650–655. <https://doi.org/10.1126/science.abc6952>.

Chu, H., Hu, B., Huang, X., Chai, Y., Zhou, D., Wang, Y., Shuai, H., Yang, D., Hou, Y., Zhang, X., et al. (2021). Host and viral determinants for efficient SARS-CoV-2 infection of the human lung. *Nat. Commun.* 12, 134. <https://doi.org/10.1038/s41467-020-20457-w>.

Davies, N.G., Abbott, S., Barnard, R.C., Jarvis, C.I., Kucharski, A.J., Munday, J.D., Pearson, C.A.B., Russell, T.W., Tully, D.C., Washburne, A.D., et al. (2021). Estimated transmissibility and impact of SARS-CoV-2 lineage B.1.1.7 in England. *Science* 372, eabg3055. <https://doi.org/10.1126/science.abg3055>.

Dodev, T.S., Karagiannis, P., Gilbert, A.E., Josephs, D.H., Bowen, H., James, L.K., Bax, H.J., Beavil, R., Pang, M.O., Gould, H.J., and Beavil, A.J. (2014). A tool kit for rapid cloning and expression of recombinant antibodies. *Sci. Rep.* 4, 5885. <https://doi.org/10.1038/srep05885>.

Faria, N.R., Mellan, T.A., Whittaker, C., Claro, I.M., Candido, D.D.S., Mishra, S., Crispim, M.A.E., Sales, F.C.S., Hawryluk, I., McCrone, J.T., et al. (2021). Genomics and epidemiology of the P.1 SARS-CoV-2 lineage in Manaus, Brazil. *Science* 372, 815–821. <https://doi.org/10.1126/science.abh2644>.

Fehr, A.R., Athmer, J., Channappanavar, R., Phillips, J.M., Meyerholz, D.K., and Perlman, S. (2015). The nsp3 macrodomain promotes virulence in mice with coronavirus-induced encephalitis. *J. Virol.* 89, 1523–1536. <https://doi.org/10.1128/JVI.02596-14>.

Fernandez, A. (2020). Structural impact of mutation D614G in SARS-CoV-2 spike protein: enhanced infectivity and therapeutic opportunity. *ACS Med. Chem. Lett.* 11, 1667–1670. <https://doi.org/10.1021/acsmchemlett.0c00410>.

Gallagher, T.M. (1997). A role for naturally occurring variation of the murine coronavirus spike protein in stabilizing association with the cellular receptor. *J. Virol.* 71, 3129–3137. <https://doi.org/10.1128/JVI.71.4.3129-3137.1997>.

Gobeil, S.M.C., Janowska, K., McDowell, S., Mansouri, K., Parks, R., Stalls, V., Kopp, M.F., Manne, K., Li, D., Wiehe, K., et al. (2021). Effect of natural mutations of SARS-CoV-2 on spike structure, conformation, and antigenicity. *Science* 373. <https://doi.org/10.1126/science.abi6226>.

Godfraind, C., Langreth, S.G., Cardellicchio, C.B., Knobler, R., Coutelier, J.P., Dubois-Dalq, M., and Holmes, K.V. (1995). Tissue and cellular distribution of an adhesion molecule in the carcinoembryonic antigen family that serves as a receptor for mouse hepatitis virus. *Lab Invest.* 73, 615–627.

Graham, C., Seow, J., Huettner, I., Khan, H., Kouphou, N., Acors, S., Winstone, H., Pickering, S., Galao, R.P., Dupont, L., et al. (2021). Neutralization potency of monoclonal antibodies recognizing dominant and subdominant epitopes on SARS-CoV-2 Spike is impacted by the B.1.1.7 variant. *Immunity* 54, 1276–1289.e6. <https://doi.org/10.1016/j.immuni.2021.03.023>.

Hensley, L.E., Holmes, K.V., Beauchemin, N., and Baric, R.S. (1998). Virus-receptor interactions and interspecies transfer of a mouse hepatitis virus. *Adv. Exp. Med. Biol.* 440, 33–41. [https://doi.org/10.1007/978-1-4615-5331-1\\_5](https://doi.org/10.1007/978-1-4615-5331-1_5).

Hoffmann, M., Hofmann-Winkler, H., and Pöhlmann, S. (2018). Priming time: how cellular proteases arm coronavirus spike proteins. In *Activation of Viruses by Host Proteases*, Eva Böttcher-Friebertshäuser, Wolfgang Garten, and Dieter Klenk Hans, eds. (Springer International Publishing), pp. 71–98.

Hoffmann, M., Kleine-Weber, H., and Pöhlmann, S. (2020). A multibasic cleavage site in the spike protein of SARS-CoV-2 is essential for infection of human lung cells. *Mol. Cell* 78, 779–784.e5. <https://doi.org/10.1016/j.molcel.2020.04.022>.

Hou, Y.J., Chiba, S., Halfmann, P., Ehre, C., Kuroda, M., Dinno, K.H., 3rd, Leist, S.R., Schafer, A., Nakajima, N., Takahashi, K., et al. (2020). SARS-CoV-2 D614G variant exhibits efficient replication ex vivo and transmission in vivo. *Science* 370, 1464–1468. <https://doi.org/10.1126/science.abe8499>.

Jackson, C.B., Farzan, M., Chen, B., and Choe, H. (2022). Mechanisms of SARS-CoV-2 entry into cells. *Nat. Rev. Mol. Cell Biol.* 23, 3–20. <https://doi.org/10.1038/s41580-021-00418-x>.

Johnson, B.A., Xie, X., Bailey, A.L., Kalveram, B., Lokugamage, K.G., Muruato, A., Zou, J., Zhang, X., Juelich, T., Smith, J.K., et al. (2021). Loss of furin cleavage site attenuates SARS-CoV-2 pathogenesis. *Nature* 597, 293–299. <https://doi.org/10.1038/s41586-021-03237-4>.

Kemp, S.A., Collier, D.A., Datir, R.P., Ferreira, I., Gayed, S., Jahun, A., Hosmillo, M., Rees-Spear, C., Mlcochova, P., Lumb, I.U., et al.; The COVID-19 Genomics UK COG-UK Consortium (2021). SARS-CoV-2 evolution during treatment of chronic infection. *Nature* 592, 277–282. <https://doi.org/10.1038/s41586-021-03291-y>.

Kumar, B., Hawkins, G.M., Kicmal, T., Qing, E., Timm, E., and Gallagher, T. (2021). Assembly and entry of severe acute respiratory syndrome coronavirus 2 (SARS-CoV2): evaluation using virus-like particles. *Cells* 10, 853. <https://doi.org/10.3390/cells10040853>.

Lau, S.Y., Wang, P., Mok, B.W.Y., Zhang, A.J., Chu, H., Lee, A.C.Y., Deng, S., Chen, P., Chan, K.H., Song, W., et al. (2020). Attenuated SARS-CoV-2 variants with deletions at the S1/S2 junction. *Emerg. Microbes Infect.* 9, 837–842. <https://doi.org/10.1080/22221751.2020.1756700>.

Lempp, F.A., Soriaga, L.B., Montiel-Ruiz, M., Benigni, F., Noack, J., Park, Y.J., Bianchi, S., Walls, A.C., Bowen, J.E., Zhou, J., et al. (2021). Lectins enhance SARS-CoV-2 infection and influence neutralizing antibodies. *Nature* 598, 342–347. <https://doi.org/10.1038/s41586-021-03925-1>.

Linsenmeyer, K., Charness, M.E., O'Brien, W.J., Strymish, J., Doshi, S.J., Ljaamo, S.K., and Gupta, K. (2021). Vaccination status and the detection of SARS-CoV-2 infection in Health care personnel under surveillance in long-term residential facilities. *JAMA Netw. Open* 4, e2134229. <https://doi.org/10.1001/jamanetworkopen.2021.34229>.

Liu, C., Mendonca, L., Yang, Y., Gao, Y., Shen, C., Liu, J., Ni, T., Ju, B., Liu, C., Tang, X., et al. (2020). The Architecture of inactivated SARS-CoV-2 with post-fusion spikes revealed by cryo-EM and cryo-ET. *Structure* 28, 1218–1224.e4. <https://doi.org/10.1016/j.str.2020.10.001>.

Matsuyama, S., and Taguchi, F. (2009). Two-step conformational changes in a coronavirus envelope glycoprotein mediated by receptor binding and proteolysis. *J. Virol.* 83, 11133–11141. <https://doi.org/10.1128/JVI.00959-09>.

McCallum, M., De Marco, A., Lempp, F.A., Tortorici, M.A., Pinto, D., Walls, A.C., Beltramello, M., Chen, A., Liu, Z., Zatta, F., et al. (2021). N-terminal domain antigenic mapping reveals a site of vulnerability for SARS-CoV-2. *Cell* 184, 2332–2347.e16. <https://doi.org/10.1016/j.cell.2021.03.028>.

Millet, J.K., and Whittaker, G.R. (2018). Physiological and molecular triggers for SARS-CoV membrane fusion and entry into host cells. *Virology* 517, 3–8. <https://doi.org/10.1016/j.virol.2017.12.015>.

Muhsen, K., Maimon, N., Mizrahi, A., Bodenheimer, O., Cohen, D., Maimon, M., Grotto, I., and Dagan, R. (2021). Effectiveness of BNT162b2 mRNA coronavirus disease 2019 (COVID-19) vaccine against Acquisition of severe acute respiratory syndrome coronavirus 2 (SARS-CoV-2) Among Healthcare workers in long-term care facilities: a prospective cohort study. *Clin. Infect. Dis.*, ciab918. <https://doi.org/10.1093/cid/ciab918>.

Muus, C., Luecken, M.D., Eraslan, G., Sikkema, L., Waghray, A., Heimberg, G., Kobayashi, Y., Vaishnav, E.D., Subramanian, A., Smillie, C., et al. (2021). Single-cell meta-analysis of SARS-CoV-2 entry genes across tissues and demographics. *Nat. Med.* 27, 546–559. <https://doi.org/10.1038/s41591-020s4101227-z>.

Nakayama, T., Lee, I.T., Jiang, S., Matter, M.S., Yan, C.H., Overdevest, J.B., Wu, C.T., Goltsev, Y., Shih, L.C., Liao, C.K., et al. (2021). Determinants of SARS-CoV-2 entry and replication in airway mucosal tissue and susceptibility

- in smokers. *Cell Rep. Med.* 2, 100421. <https://doi.org/10.1016/j.xcrm.2021.100421>.
- Ng, O.T., Koh, V., Chiew, C.J., Marimuthu, K., Thevasagayam, N.M., Mak, T.M., Chua, J.K., Ong, S.S.H., Lim, Y.K., Ferdous, Z., et al. (2021). Impact of delta variant and vaccination on SARS-CoV-2 secondary attack rate among household close contacts. *Lancet Reg. Health West. Pac.* 17, 100299. <https://doi.org/10.1016/j.lanwpc.2021.100299>.
- Niu, S., Wang, J., Bai, B., Wu, L., Zheng, A., Chen, Q., Du, P., Han, P., Zhang, Y., Jia, Y., et al. (2021). Molecular basis of cross-species ACE2 interactions with SARS-CoV-2-like viruses of pangolin origin. *EMBO J.* 40, e107786. <https://doi.org/10.15252/embj.2021107786>.
- Park, J.E., Li, K., Barlan, A., Fehr, A.R., Perlman, S., McCray, P.B., Jr., and Gallagher, T. (2016). Proteolytic processing of Middle East respiratory syndrome coronavirus spikes expands virus tropism. *Proc. Natl. Acad. Sci. U S A.* 113, 12262–12267. <https://doi.org/10.1073/pnas.1608147113>.
- Peacock, T.P., Brown, J.C., Zhou, J., Thakur, N., Newman, J., Kugathasan, R., Sukhova, K., Kaforou, M., Bailey, D., and Barclay, W.S. (2022). The SARS-CoV-2 variant, Omicron, shows rapid replication in human primary nasal epithelial cultures and efficiently uses the endosomal route of entry. Preprint at bioRxiv. <https://doi.org/10.1101/2021.12.31.474653>.
- Peacock, T.P., Goldhill, D.H., Zhou, J., Baillon, L., Frise, R., Swann, O.C., Kugathasan, R., Penn, R., Brown, J.C., Sanchez-David, R.Y., et al. (2021). The furin cleavage site in the SARS-CoV-2 spike protein is required for transmission in ferrets. *Nat. Microbiol.* 6, 899–909. <https://doi.org/10.1038/s41564-021-00908-w>.
- Peng, R., Wu, L.A., Wang, Q., Qi, J., and Gao, G.F. (2021). Cell entry by SARS-CoV-2. *Trends Biochem. Sci.* 46, 848–860. <https://doi.org/10.1016/j.tibs.2021.06.001>.
- Peter, A.S., Roth, E., Schulz, S.R., Fraedrich, K., Steinmetz, T., Damm, D., Hauke, M., Richel, E., Mueller-Schmucker, S., Habenicht, K., et al. (2021). A pair of noncompeting neutralizing human monoclonal antibodies protecting from disease in a SARS-CoV-2 infection model. *Eur. J. Immunol.* 00, 1–14. <https://doi.org/10.1002/eji.202149374>.
- Planas, D., Veyer, D., Baidaliuk, A., Staropoli, I., Guivel-Benhassine, F., Rajah, M.M., Planchais, C., Porrot, F., Robillard, N., Puech, J., et al. (2021). Reduced sensitivity of SARS-CoV-2 variant Delta to antibody neutralization. *Nature* 596, 276–280. <https://doi.org/10.1038/s41586-021-03777-9>.
- Puray-Chavez, M., LaPak, K.M., Schrank, T.P., Elliott, J.L., Bhatt, D.P., Agajanian, M.J., Jasuja, R., Lawson, D.Q., Davis, K., Rothlauf, P.W., et al. (2021). Systematic analysis of SARS-CoV-2 infection of an ACE2-negative human airway cell. *Cell Rep.* 36, 109364. <https://doi.org/10.1016/j.celrep.2021.109364>.
- Qing, E., Hantak, M., Perlman, S., and Gallagher, T. (2020). Distinct roles for sialoside and protein receptors in coronavirus infection. *mBio* 11, e02764-19. <https://doi.org/10.1128/mBio.02764-19>.
- Qing, E., Kicmal, T., Kumar, B., Hawkins, G.M., Timm, E., Perlman, S., and Gallagher, T. (2021). Dynamics of SARS-CoV-2 spike proteins in cell entry: control elements in the amino-terminal domains. *mBio* 12, e0159021. <https://doi.org/10.1128/mBio.01590-21>.
- Ren, W., Lan, J., Ju, X., Gong, M., Long, Q., Zhu, Z., Yu, Y., Wu, J., Zhong, J., Zhang, R., et al. (2021). Mutation Y453F in the spike protein of SARS-CoV-2 enhances interaction with the mink ACE2 receptor for host adaption. *PLoS Pathog.* 17, e1010053. <https://doi.org/10.1371/journal.ppat.1010053>.
- Shang, J., Wan, Y., Liu, C., Yount, B., Gully, K., Yang, Y., Auerbach, A., Peng, G., Baric, R., and Li, F. (2020a). Structure of mouse coronavirus spike protein complexed with receptor reveals mechanism for viral entry. *PLoS Pathog.* 16, e1008392. <https://doi.org/10.1371/journal.ppat.1008392>.
- Shang, J., Wan, Y., Luo, C., Ye, G., Geng, Q., Auerbach, A., and Li, F. (2020b). Cell entry mechanisms of SARS-CoV-2. *Proc. Natl. Acad. Sci. U S A.* 117, 11727–11734. <https://doi.org/10.1073/pnas.2003138117>.
- Singanayagam, A., Hakki, S., Dunning, J., Madon, K.J., Crone, M.A., Koycheva, A., Derqui-Fernandez, N., Barnett, J.L., Whitfield, M.G., Varro, R., et al. (2022). Community transmission and viral load kinetics of the SARS-CoV-2 delta (B.1.617.2) variant in vaccinated and unvaccinated individuals in the UK: a prospective, longitudinal, cohort study. *Lancet Infect. Dis.* 22, 183–195. [https://doi.org/10.1016/S1473-3099\(21\)00648-4](https://doi.org/10.1016/S1473-3099(21)00648-4).
- Suryadevara, N., Shrihari, S., Gilchuk, P., VanBlargan, L.A., Binshtein, E., Zost, S.J., Nargi, R.S., Sutton, R.E., Winkler, E.S., Chen, E.C., et al. (2021). Neutralizing and protective human monoclonal antibodies recognizing the N-terminal domain of the SARS-CoV-2 spike protein. *Cell* 184, 2316–2331.e15. <https://doi.org/10.1016/j.cell.2021.03.029>.
- Tegally, H., Wilkinson, E., Giovanetti, M., Iranzadeh, A., Fonseca, V., Giandhari, J., Doolabh, D., Pillay, S., San, E.J., Msoni, N., et al. (2021). Detection of a SARS-CoV-2 variant of concern in South Africa. *Nature* 592, 438–443. <https://doi.org/10.1038/s41586-021-03402-9>.
- Volz, E., Hill, V., McCrone, J.T., Price, A., Jorgensen, D., O’Toole, A., Southgate, J., Johnson, R., Jackson, B., Nascimento, F.F., et al. (2021). Evaluating the effects of SARS-CoV-2 spike mutation D614G on transmissibility and pathogenicity. *Cell* 184, 64–75.e11. <https://doi.org/10.1016/j.cell.2020.11.020>.
- Walls, A.C., Park, Y.J., Tortorici, M.A., Wall, A., McGuire, A.T., and Veesler, D. (2020). Structure, function, and antigenicity of the SARS-CoV-2 spike glycoprotein. *Cell* 181, 281–292.e6. <https://doi.org/10.1016/j.cell.2020.02.058>.
- Walls, A.C., Xiong, X., Park, Y.J., Tortorici, M.A., Snijder, J., Quispe, J., Cameron, E., Gopal, R., Dai, M., Lanzavecchia, A., et al. (2019). Unexpected receptor functional mimicry elucidates activation of coronavirus fusion. *Cell* 176, 1026–1039.e15. <https://doi.org/10.1016/j.cell.2018.12.028>.
- Wang, P., Casner, R.G., Nair, M.S., Yu, J., Guo, Y., Wang, M., Chan, J.F.W., Cerutti, G., Iketani, S., Liu, L., et al. (2022). A monoclonal antibody that neutralizes SARS-CoV-2 variants, SARS-CoV, and other sarbecoviruses. *Emerg. Microbes Infect.* 11, 147–157. <https://doi.org/10.1080/22221751.2021.2011623>.
- Wang, P., Nair, M.S., Liu, L., Iketani, S., Luo, Y., Guo, Y., Wang, M., Yu, J., Zhang, B., Kwong, P.D., et al. (2021a). Antibody resistance of SARS-CoV-2 variants B.1.351 and B.1.1.7. *Nature* 593, 130–135. <https://doi.org/10.1038/s41586-021-03398-2>.
- Wang, R., Zhang, Q., Ge, J., Ren, W., Zhang, R., Lan, J., Ju, B., Su, B., Yu, F., Chen, P., et al. (2021b). Analysis of SARS-CoV-2 variant mutations reveals neutralization escape mechanisms and the ability to use ACE2 receptors from additional species. *Immunity* 54, 1611–1621.e5. <https://doi.org/10.1016/j.immuni.2021.06.003>.
- Wei, C., Wan, L., Yan, Q., Wang, X., Zhang, J., Yang, X., Zhang, Y., Fan, C., Li, D., Deng, Y., et al. (2020). HDL-scavenger receptor B type 1 facilitates SARS-CoV-2 entry. *Nat. Metab.* 2, 1391–1400. <https://doi.org/10.1038/s42255-020-00324-0>.
- Willett, B.J., Grove, J., MacLean, O.A., Wilkie, C., Logan, N., Lorenzo, G.D., Furnon, W., Scott, S., Manali, M., Szemiel, A., et al. (2022). The hyper-transmissible SARS-CoV-2 Omicron variant exhibits significant antigenic change, vaccine escape and a switch in cell entry mechanism. Preprint at medRxiv. <https://doi.org/10.1101/2022.01.03.21268111>.
- Wrapp, D., Wang, N., Corbett, K.S., Goldsmith, J.A., Hsieh, C.L., Abiona, O., Graham, B.S., and McLellan, J.S. (2020). Cryo-EM structure of the 2019-nCoV spike in the prefusion conformation. *Science* 367, 1260–1263. <https://doi.org/10.1126/science.abb2507>.
- Yang, Z., Wang, Y., Jin, Y., Zhu, Y., Wu, Y., Li, C., Kong, Y., Song, W., Tian, X., Zhan, W., et al. (2021). A non-ACE2 competing human single-domain antibody confers broad neutralization against SARS-CoV-2 and circulating variants. *Signal Transduct. Target Ther.* 6, 378. <https://doi.org/10.1038/s41392-021-00810-1>.
- Yurkovetskiy, L., Wang, X., Pascal, K.E., Tomkins-Tinch, C., Nyallie, T.P., Wang, Y., Baum, A., Diehl, W.E., Dauphin, A., Carbone, C., et al. (2020). Structural and functional analysis of the D614G SARS-CoV-2 spike protein variant. *Cell* 183, 739–751.e8. <https://doi.org/10.1016/j.cell.2020.09.032>.
- Zhang, J., Cai, Y., Xiao, T., Lu, J., Peng, H., Sterling, S.M., Walsh, R.M., Jr., Rits-Volloch, S., Zhu, H., Woosley, A.N., et al. (2021a). Structural impact on

SARS-CoV-2 spike protein by D614G substitution. *Science* 372, 525–530. <https://doi.org/10.1126/science.abf2303>.

Zhang, L., Jackson, C.B., Mou, H., Ojha, A., Peng, H., Quinlan, B.D., Rangarajan, E.S., Pan, A., Vanderheiden, A., Suthar, M.S., et al. (2020). SARS-CoV-2 spike-protein D614G mutation increases virion spike density and

infectivity. *Nat. Commun.* 11, 6013. <https://doi.org/10.1038/s41467-020-19808-4>.

Zhang, W., Davis, B.D., Chen, S.S., Sincuir Martinez, J.M., Plummer, J.T., and Vail, E. (2021b). Emergence of a novel SARS-CoV-2 variant in southern California. *JAMA* 325, 1324–1326. <https://doi.org/10.1001/jama.2021.1612>.

## STAR★METHODS

### KEY RESOURCES TABLE

REAGENT or RESOURCE	SOURCE	IDENTIFIER
<b>Antibodies</b>		
rabbit polyclonal anti-SARS-CoV-2-S1	SinoBiological	Cat#40591-T62
rabbit polyclonal anti-SARS-S2	Dr. Carolyn Machamer	JH50520001
mouse monoclonal anti-SARS-S2	ThermoFisher	Cat#MA5-35946
goat anti-human IgG	Santa Cruz Biotechnologies	Cat#sc-2453
rabbit monoclonal anti-hACE2	Invitrogen	Cat# MA5-32307
4A8	(Chi et al., 2020), and this paper	N/A
TRES328	Dr. Hans-Martin Jäck (Peter et al., 2021)	N/A
Goat Anti-Rabbit IgG - HRP	Perkin Elmer	Cat#NEF812001EA
<b>Bacterial and virus strains</b>		
SARS-CoV (MA15)	K. Subbarao	N/A
SARS-CoV-2 (D614G)	This paper	N/A
<b>Chemicals, peptides, and recombinant proteins</b>		
LipoD293	SigmaGen	Cat#SL100668
Amicon Ultra-15 100 NMWL, kDa	Millipore	Cat#UFC910024
qEVoriginal / 35 nm	Izon	N/A
Nano-Glo HiBIT Extracellular Detection System	Promega	Cat#N2420
TPCK Trypsin Treated from Bovine Pancreas	Sigma	Cat#T1426-50MG
HiTrap Protein A High Performance Columns	GE Healthcare	Cat#GE17-0402-01
HRP Conjugation Kit - Lightning Link	Abcam	Cat#ab102890
<b>Experimental models: Cell lines</b>		
HEK293T	Dr. Edward Campbell	N/A
Vero-E6	ATCC	Cat#CRL-1586
<b>Recombinant DNA</b>		
WT-SARS-CoV-2 BAC	Drs. Sonja Zuniga and Luis Enjuanes	N/A
pVITRO1-M80-F2-IgG1/ $\kappa$	Andrew Beavil (Dodev et al., 2014)	Addgene plasmid # 50383
pCEP4-hACE2-Fc	(Qing et al., 2021)	N/A
pCEP4-mCEACAM-Fc	(Gallagher, 1997)	N/A
pcDNA3.1-MCS	Invitrogen	Cat#V79020
pcDNA3.1-SARS-CoV-S	(Qing et al., 2021)	GenBank: AY278741.1
pcDNA3.1-SARS-CoV-S (SARS-2 NTD loops)	(Qing et al., 2021)	N/A
pcDNA3.1-SARS-CoV-2-S	(Kumar et al., 2021)	GenBank: NC_045512.2
pcDNA3.1-SARS-CoV-2-E	(Kumar et al., 2021)	GenBank: NC_045512.2
pcDNA3.1-SARS-CoV-2-M	(Kumar et al., 2021)	GenBank: NC_045512.2
pcDNA3.1-SARS-CoV-2-N	(Kumar et al., 2021)	GenBank: NC_045512.2
pcDNA3.1-SARS-CoV-2-HiBIT-N	(Kumar et al., 2021)	N/A
pcDNA3.1-SARS-CoV-2-S (D614G)	(Qing et al., 2021)	N/A
pcDNA3.1-SARS-CoV-2-S (D614G, SARS-1 NTD loops)	(Qing et al., 2021)	N/A
pcDNA3.1-SARS-CoV-2-S ( $\Delta$ PRRA)	This paper	N/A
pcDNA3.1-SARS-CoV-2-S (D614G, $\Delta$ PRRA)	This paper	N/A

(Continued on next page)

**Continued**

REAGENT or RESOURCE	SOURCE	IDENTIFIER
pcDNA3.1-SARS-CoV-2-S (D614G, 2P)	This paper	N/A
pcDNA3.1-SARS-CoV-2-S (D614G, D737A)	This paper	N/A
pcDNA3.1-SARS-CoV-2-S (D614G, N317A)	This paper	N/A
pcDNA3.1-SARS-CoV-2-S (D614G, D796H)	This paper	N/A
pcDNA3.1-SARS-CoV-2-S (D614G, D796Y)	This paper	N/A
pcDNA3.1-SARS-CoV-2-S (D614G, A701P/N703P)	This paper	N/A
pcDNA3.1-SARS-CoV-2-S (D614G, $\alpha$ -NTD)	This paper	N/A
pcDNA3.1-SARS-CoV-2-S (D614G, $\beta$ -NTD)	This paper	N/A
pcDNA3.1-SARS-CoV-2-S (D614G, $\gamma$ -NTD)	This paper	N/A
pcDNA3.1-SARS-CoV-2-S (D614G, $\delta$ -NTD)	This paper	N/A
pcDNA3.1-SARS-CoV-2-S (D614G, o-NTD)	This paper	N/A
pCMV-LgBiT	Promega	Cat#N2681
pcDNA3.1-hACE2-LgBiT	(Kumar et al., 2021)	N/A
<b>Software and algorithms</b>		
AlphaView	ProteinSimple	N/A
PyMOL	Schrödinger	N/A
Prism	GraphPad	N/A

**RESOURCE AVAILABILITY**

**Lead contact**

Requests for further information or resources and reagents should be directed to the lead contact, Tom Gallagher ([tgallag@luc.edu](mailto:tgallag@luc.edu)).

**Materials availability**

All materials generated in this study will be made available on request by the Lead Contact.

**Data and code availability**

- All data reported in this paper will be shared by the [lead contact](#) upon request.
- This paper does not report original code.
- Any additional information required to reanalyze the data reported in this paper is available from the [lead contact](#) upon request.

**EXPERIMENTAL MODEL AND SUBJECT DETAILS**

**Cell lines**

HEK293T (obtained from Dr. Ed Campbell, Loyola University Chicago) and Vero-E6 (ATCC CRL-1586) cells were maintained in DMEM-10% FBS [Dulbecco's Modified Eagle Media (DMEM) containing 10 mM HEPES, 100 nM sodium pyruvate, 0.1 mM non-essential amino acids, 100 U/mL penicillin G, and 100  $\mu$ g/mL streptomycin, and supplemented with 10% fetal bovine serum (FBS, Atlanta Biologicals)]. All cell lines were cultured in a 5% CO<sub>2</sub> incubator at 37°C.

**Viruses**

SARS-CoV (MA15), a gift from K. Subbarao (National Institutes of Health, Bethesda, MD), was propagated on Vero E6 cells. SARS-CoV-2 D614G was obtained by modifying WT-SARS-CoV-2 BAC (a gift from Drs. Sonja Zuniga and Luis Enjuanes, CNB-CSIC, Madrid, Spain) via reverse engineering (Fehr et al., 2015). SARS-CoV-2 D614G was resurrected by transfecting WT-SARS-CoV-2 (D614G) BAC into Vero E6 cells, and plaque purified and sequence verified subsequently.

**METHOD DETAILS**

**Plasmid construction**

Full-length SARS-CoV S (GenBank: AY278741.1) and SARS-CoV-2 S, E, M, and N (GenBank: NC\_045512.2) genes were synthesized by Genscript, Inc. as human codon-optimized cDNAs, and inserted into pcDNA3.1 expression vectors. All S mutations were

introduced via site-directed mutagenesis, except for omicron NTD, which was synthesized (Integrated DNA Technologies). HiBiT-N was constructed by fusing HiBiT peptide (VSGWRLFKKIS) coding sequences with linker (GSSGGSSG) to the 5' end of the N gene, as described in (Kumar et al., 2021; Qing et al., 2021). The pCMV-LgBiT expression plasmid was purchased from Promega. pcDNA3.1-hACE2-C9 was obtained from Dr. Michael Farzan, Scripps Florida. pcDNA3.1-hACE2-LgBiT was constructed by fusing the coding sequence of LgBiT to the 3' end of hACE2 gene.

### Western blot and antibodies

Samples in SDS solubilizer [0.0625 M Tris-HCl (pH 6.8), 10% glycerol, 0.01% bromophenol blue, 2% (wt/vol) SDS, +/- 2% 2-mercaptoethanol] were heated at 95°C for 5 min, electrophoresed through 8% or 10% (wt/vol) polyacrylamide-SDS gels, transferred to nitrocellulose membranes (Bio-Rad), and incubated with rabbit polyclonal anti-SARS-CoV-2-S1 (SinoBiological, cat: 40591-T62), rabbit polyclonal anti-SARS-S2 (#JH50520001, obtained from Dr. Carolyn Machamer, Johns Hopkins University), mouse monoclonal anti-SARS-S2 (ThermoFisher, cat: MA5-35946, conjugated to HRP), goat anti-human IgG (sc-2453, Santa Cruz Biotechnologies), rabbit monoclonal anti-hACE2 (Invitrogen, cat: MA5-32307), or purified LgBiT-substrate cocktail (Promega). After incubation with appropriate HRP-tagged secondary antibodies and chemiluminescent substrate (Thermo Fisher), the blots were imaged and processed with a FlourChem E (Protein Simple).

Recombinant 4A8 was synthesized by using its published VH and VL sequences (Chi et al., 2020) to replace their counterparts in pVITRO1-M80-F2-IgG1/ $\kappa$  (a gift from Andrew Beavil, Addgene plasmid # 50383; <http://n2t.net/addgene:50383>; RRID:Addgene\_50383, (Dodev et al., 2014)). TRES328 (Peter et al., 2021) was obtained from Dr. Hans-Martin Jäck, Friedrich-Alexander-Universität.

### Plaque reduction assay

Circa 50 pfu of authentic SARS-CoV or SARS-CoV-2 (D614G) was incubated with titrated levels of 4A8 for 30 min at 37°C. The virus-antibody mixture was then inoculated onto Vero-E6 cells for 1 h at 37°C, and media were replaced with DMEM-2% FBS and incubated at 37°C. Plaques were counted at 48 hpi, and plaque reduction quantified relative to vehicle control.

### Virus-like particles (VLPs)

HiBiT-N tagged VLPs were produced as described previously (Kumar et al., 2021; Qing et al., 2021). Briefly, equimolar amounts of full-length CoV S, E (envelope), M (membrane) and HiBiT-N encoding plasmids (total 10  $\mu$ g) were LipoD (SigmaGen, cat: SL100668)-transfected into 10<sup>7</sup> HEK293T cells. To produce spikeless “No S” VLPs, the S expression plasmids were replaced with empty vector plasmids. At 6 h post-transfection, cells were replenished with fresh DMEM-10% FBS. HiBiT-N VLPs were collected in FBS-free DMEM from 24 to 48 h post-transfection. FBS-free DMEM containing HiBiT-N VLPs were clarified by centrifugation (300xg, 4°C, 10 min; 3000xg, 4°C, 10 min).

To obtain purified viral particles, clarified VLP-containing FBS-free DMEM was concentrated 100-fold by ultrafiltration (Amicon, 100 kDa) and then VLPs were purified using size-exclusion chromatography (SEC qEV original, Izon, Inc., usage following product instructions). VLPs were eluted from columns into 2x FBS-free DMEM. Peak VLP fractions were identified after detergent lysis of VLPs by adding LgBiT and measuring complemented Nluc in a luminometer. For downstream experiments, VLP inputs were normalized based on their Nluc activity upon LgBiT complementation. Peak fractions were stored at -80°C.

### Cell-free fusion assay

hACE2-LgBiT EVs were obtained as described previously (Qing et al., 2021). Briefly, HEK293T target cells were LipoD-transfected with pcDNA3.1-hACE2-LgBiT. At 6 h post-transfection, transfection media were removed, rinsed, and replaced with FBS-free DMEM. Media were collected at 48 h post-transfection, clarified (300xg, 4°C, 10 min; 3000xg, 4°C, 10 min), and concentrated 100-fold by ultrafiltration (Amicon, 100 kDa). EVs were then purified using size-exclusion chromatography (qEV original, Izon, Inc.) using PBS pH 7.4 as eluant. Peak EV fractions were identified by adding HiBiT-containing detergent and subsequent Nluc measurement by luminometry. EVs were stored at 4°C.

Cell-free fusion assays were performed as described previously (Qing et al., 2021). Briefly, at 4°C, equal volumes of HiBiT-N VLPs and hACE2-LgBiT EVs were mixed with nanoluc substrate (cat#N2420, Promega) and trypsin (Sigma; 10 ng/ $\mu$ L or as indicated) in 384-well multiwell plates. Sample plates were then loaded into a Glomax luminometer maintained at 37°C. Nluc accumulations were recorded over time. VLP-EV cell-free fusions were quantified as the fold increase of Nluc signal from S-bearing VLPs over the signal from spikeless (No S) VLP background control.

For antibody neutralization assays, VLPs were incubated with serial dilutions of either 4A8, mCEACAM-Fc, or TRES328 for 30 min at 37°C before adding hACE2-LgBiT EVs, substrate, and trypsin. For proteolytic activation assays, VLPs were incubated with hACE2-LgBiT EVs for 30 min at 37°C before adding substrate and serial dilutions of trypsin.

### VLP S1-retention assay

SARS-CoV-2 S (D614G) VLPs were incubated with vehicle or 4A8 (400 nM) for 30 min at 37°C. Then vehicle, hACE2-Fc (400 nM), or mCEACAM-Fc (400 nM) were added and the mixtures were incubated for 24 h at 37°C. After incubation, the VLPs were density purified from the mixture through a 20% sucrose cushion (SW60, 35000 rpm, 2 h, 4°C). The resulted pellets were resuspended and each

split into two halves, one half was probed with anti-S1 antibody while the other half with anti-S2 antibody. S1-S2 ratios were calculated from the Western blot band intensities.

### S2' cleavage assay

VLPs bearing SARS-2-S (D614G) or SARS-1/2-S, or recombinant SARS-CoV-2 (D614G) were incubated with vehicle, 4A8 (500 nM), mCEACAM-Fc (500 nM), or TRES328 (500 nM) for 30 min at 37°C. Subsequently, hACE2-LgBiT EVs were added and incubated for 30 min at 37°C. Lastly, titrated levels of trypsin were added and incubated for 30 min at 37°C. A portion of the resulting mixture was mixed with Niluc substrate and fusion was measured by ways of RLU. SDS-solubilizer was added to the rest of the mixture for Western blot analysis.

### Fc constructs

pCEP4-mCEACAM-Fc was constructed previously (Gallagher, 1997). pCEP4-hACE2-Fc was generated using the strategy described in (Qing et al., 2020). Briefly, the mCEACAM coding region was removed by NotI and MreI digestion, and replaced with hACE2 ectodomain (codons 1–740). The expression plasmids were LipoD-transfected into HEK293T cells, and transfected cells were incubated in FBS-free DMEM containing 2% (wt/vol) Cell Boost 5 (Hyclone). Conditioned media were collected on days 4 and 7, clarified free of debris (300xg, 4°C, 10 min; 4500xg, 4°C, 10 min), and Fc-tagged proteins then purified using HiTrap Protein A High Performance Columns (GE Healthcare) according to the manufacturer instructions. Purified proteins were dialyzed in PBS [pH 7.4], quantified spectrophotometrically and stored at -20°C until use.

## QUANTIFICATION AND STATISTICAL ANALYSIS

All Western blot images are representative of three or four biological repeats (depending on the experiment, specified in the figure legends). The pixel density of the relevant bands were quantified by AlphaView (ProteinSimple). The raw pixel values (or ratios) were subsequently normalized to their corresponding vehicle control, whose values were set to one. Mean and SEM are shown based on data from biological repeats.

All antibody titration and trypsin titration graphs are one representative of three biological repeats. For these graphs, mean and SD are shown based on three technical replicates. To quantitatively compare the effects of spike mutations on antibody response or protease sensitivity, the antibody IC<sub>50</sub> or trypsin EC<sub>50</sub> values from each biological replicate were pooled, and subsequently normalized to their corresponding WT spike control, whose IC<sub>50</sub> or EC<sub>50</sub> values were set to one. Mean and SEM are shown based on data from biological repeats.

For instances where only one pair of conditions were compared, statistical analyses were done using one-sample *t*-tests. For instances where multiple pairs of conditions were compared, one-way analysis of variance followed by the appropriate post hoc tests were applied. Tests used for each dataset are specified in the figure legends. All graphs and statistical analyses were completed using Prism 8 (GraphPad). *p*-values less than 0.05 were considered statistically significant.